Acta Crystallographica Section D
Biological Crystallography
ISSN 0907-4449

Structural insights into the assembly of the human and archaeal signal recognition particles

Klemens Wild,* Gert Bange, Gunes Bozkurt, Bernd Segnitz, Astrid Hendricks and Irmgard Sinning

Heidelberg University Biochemistry Center (BZH), University of Heidelberg, INF328, D-69120 Heidelberg, Germany

Correspondence e-mail: klemens.wild@bzh.uni-heidelberg.de

Received 13 November 2009
Accepted 7 January 2010

PDB References: SRP19–SRP RNA complexes, human, 3ktv; *Sulfolobus solfataricus*, 3ktw.

The signal recognition particle (SRP) is a conserved ribonucleoprotein (RNP) complex that co-translationally targets membrane and secretory proteins to membranes. The assembly of the particle depends on the proper folding of the SRP RNA, which in mammalia and archaea involves an induced-fit mechanism within helices 6 and 8 in the S domain of SRP. The two helices are juxtaposed and clamped together upon binding of the SRP19 protein to their apices. In the current assembly paradigm, archaeal SRP19 causes the asymmetric loop of helix 8 to bulge out and expose the binding platform for the key player SRP54. Based on a heterologous archaeal SRP19–human SRP RNA structure, mammalian SRP19 was thought not to be able to induce this change, thus explaining the different requirements of SRP19 for SRP54 recruitment. In contrast, the crystal structures of a crenarchaeal and the all-human SRP19–SRP RNA binary complexes presented here show that the asymmetric loop is bulged out in both binary complexes. Differences in SRP assembly between mammalia and archaea are therefore independent of SRP19 and are based on differences in SRP RNA itself. A new SRP-assembly scheme is presented.

1. Introduction

The signal recognition particle (SRP) is a conserved ribonucleoprotein (RNP) complex that is responsible for the co-translational targeting of proteins destined for membrane insertion or secretion (Cross *et al.*, 2009; Egea *et al.*, 2005; Nagai *et al.*, 2003). SRP recognizes hydrophobic N-terminal signal sequences as soon as they emerge from the ribosomal polypeptide exit tunnel. The ribosome–nascent chain complex (RNC) is transferred to the translocation channel located in the endoplasmic reticulum membrane in eukarya, in the plasma membrane in bacteria and archaea or, in the special case of chloroplasts, in the thylakoid membrane. Productive protein targeting is ensured by guanosine triphosphate (GTP) hydrolysis within SRP and its membrane-attached receptor (SR; Grudnik *et al.*, 2009).

The universally conserved SRP core responsible for signal recognition and GTP-dependent targeting consists of a preserved stem-loop RNA structure (helix 8 in eukarya and archaea; domain IV in bacteria) bound to the multidomain SRP GTPase SRP54 [fifty-four homologue (Ffh) in bacteria] (Luirink & Sinning, 2004; Batey *et al.*, 2000; Hainzl *et al.*, 2007; Kuglstatter *et al.*, 2002; Fig. 1*a*). The SRP54 M domain (SRP54M) binds to hydrophobic signal sequences and to helix 8 of SRP RNA (Bradshaw *et al.*, 2009; Batey *et al.*, 2000), while SRP54NG forms a heterodimeric targeting complex with the SRP receptor (Egea *et al.*, 2004; Focia *et al.*, 2004). In mammalia and archaea, the SRP core is extended to form the

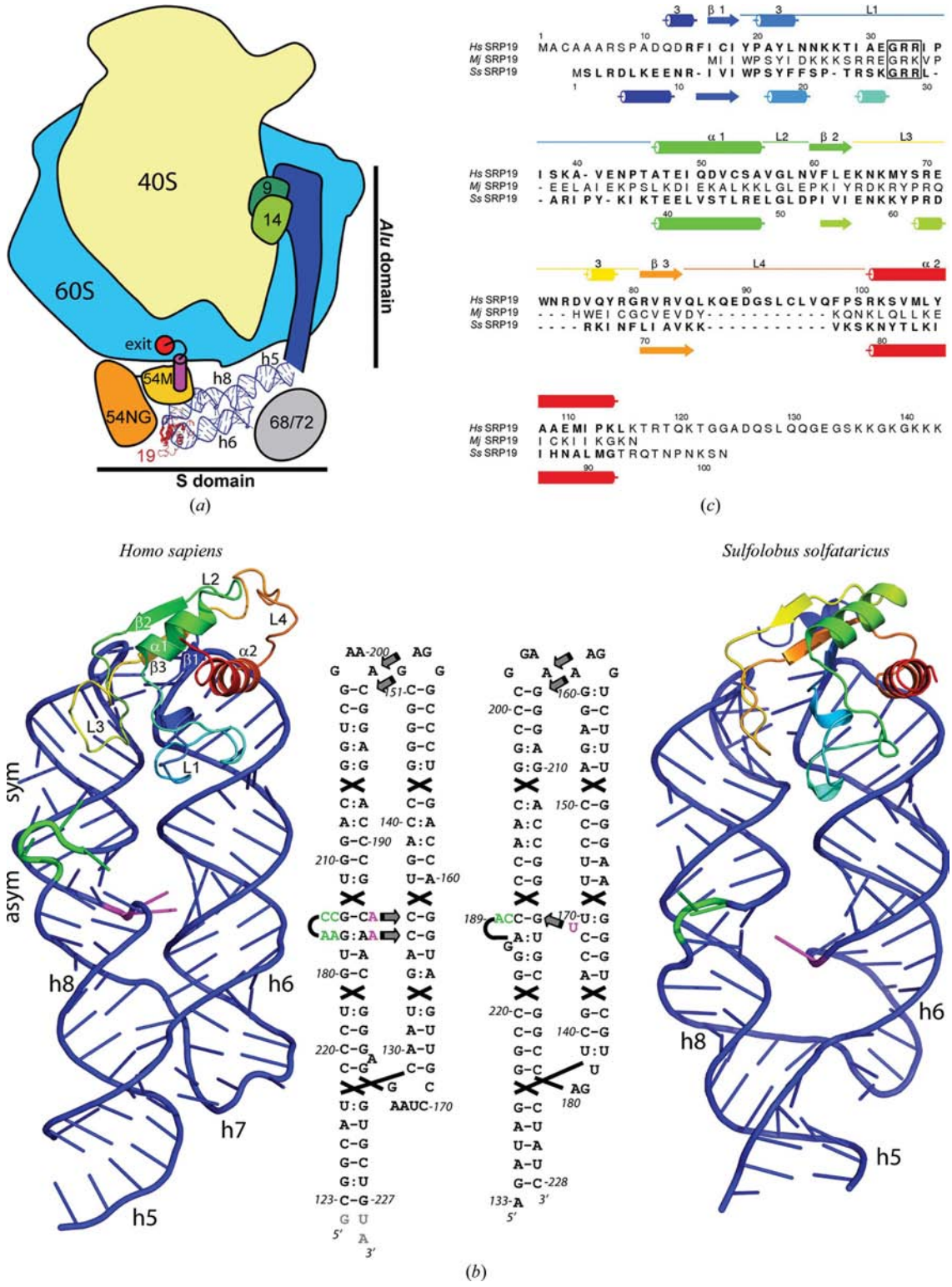

Figure 1
SRP19–SRP RNA binary complexes. (*a*) Context of the binary complex with respect to the entire mammalian ribosome–nascent chain/SRP targeting complex (shown in a scheme derived from PDB entry 2j37; Halic *et al.*, 2006). Ribosomal subunits, SRP proteins (plus domains for SRP54) and RNA helices 6–8 (denoted h5–h8) and the polypeptide exit tunnel (exit) are labelled. The signal peptide is shown as a magenta cylinder. (*b*) Structures of the human and *S. solfataricus* (*Ss*) SRP19–SRP RNA binary complexes. SRP19 proteins are coloured with a colour ramp from blue to red. The positions of the symmetric (sym) and asymmetric (asym) RNA loops are indicated. The long strand of the asymmetric loop is shown in green and bulged-out nucleotides in (human) or opposite (*Ss*) the short strand of the loop are shown in magenta. Sequences and secondary structures of the corresponding SRP RNAs are shown together with RNA–RNA tertiary interactions (grey arrows). Non-native bases at the termini are shown in grey. (*c*) Structure-based sequence alignment of human (*Hs*), *M. jannaschii* (*Mj*) and *S. solfataricus* (*Ss*) SRP19 proteins. Secondary-structure elements and loops are shown (for *Hs* and *Ss*) using the same colour ramp as in (*b*) and are labelled for human SRP19. Residues included in the structures are emphasized in bold.

S domain (large domain) by a second stem-loop structure (helix 6; Rosenblad *et al.*, 2003), which is aligned parallel to helix 8 with the aid of the SRP-assembly protein SRP19 (Oubridge *et al.*, 2002; Hainzl *et al.*, 2002). The S domain is complemented by helix 5, which is connected to helices 6 and 8 of SRP RNA *via* an RNA three-way junction. In mammalian SRP, this region additionally binds to the SRP68/72 heterodimer, the structure and function of which remain unresolved (Menichelli *et al.*, 2007). Mammalian and archaeal SRPs are completed by the *Alu* domain, which has been shown in mammalia to be responsible for the elongation-arrest function of SRP (Siegel & Walter, 1986) and consists of the SRP9/14 heterodimer bound to the 5′ and 3′ ends of SRP RNA (∼300 nucleotides in total; Weichenrieder *et al.*, 2000).

With the exception of the chloroplast system, SRP is an RNP complex, raising the question of how the particle is assembled. RNP assembly has been studied for SRP systems from all domains of life (Diener & Wilson, 2000; Menichelli *et al.*, 2007; Rose & Weeks, 2001; Batey *et al.*, 2001; Sauer-Eriksson & Hainzl, 2003). Eukaryotic SRP is assembled in distinct cellular compartments (Maity *et al.*, 2006). All SRP proteins except SRP54 are imported into the nucleus to bind SRP RNA (Politz *et al.*, 2000; Jacobson & Pederson, 1998), whereupon the complex is exported back to the cytoplasm to associate with SRP54. This 'SRP54-late' assembly has been shown to be necessary to avoid misassembly of the particle (Maity & Weeks, 2007). In contrast, archaeal and bacterial SRPs fold in the cytosol and late binding of SRP54 seems not to be essential. *Escherichia coli* SRP comprises the simplest RNP, consisting only of Ffh bound to SRP RNA (4.5S RNA). The crystal structure of the Ffh M domain bound to domain IV of 4.5S RNA revealed metal-dependent binding to a distorted RNA minor groove consisting of four universally conserved mismatched base pairs (symmetric loop; Batey *et al.*, 2000, 2001). In addition, the M domain induces a large conformational change in the adjacent asymmetric loop, thus exposing a conserved adenosine on a platform formed by the longer proximal strand. The asymmetric loop has been found by NMR techniques to form a flexible hinge (Schmitz *et al.*, 1999) and the platform is only induced in the presence of Ffh.

The same structural principles apply to the human and archaeal SRP core (SRP54 and helix 8). However, the SRP core is connected to SRP19 bound to helix 6 and its assembly and structural rearrangements have been found to be more complex (Sauer-Eriksson & Hainzl, 2003; Rose & Weeks, 2001; Menichelli *et al.*, 2007; Diener & Wilson, 2000). While the symmetric loop remains rigid, the conformation of the asymmetric loop is altered by tertiary interaction with the juxtaposed helix 6. These interactions are distinct in the known human and archaeal SRP S-domain structures. While in archaeal SRP (*Methanococcus jannaschii*) two adjacent adenine bases are looped-out from helix 6 to form A-minor motifs with the two base pairs next to the asymmetric loop (Hainzl *et al.*, 2007), in human SRP two adenines from the short strand of the asymmetric loop make similar interactions with a completely base-paired helix 6 (Kuglstatter *et al.*, 2002). In addition, the interactions in archaeal SRP are already present in free SRP RNA (Hainzl *et al.*, 2005), but in human SRP they are described in the current assembly paradigm to form only upon the addition of SRP54 (SRP54M; Kuglstatter *et al.*, 2002).

Here, we present X-ray structures of a first crenarchaeal and of the all-human complexes of SRP19 bound to S-domain SRP RNA (hereafter referred to as binary complexes). The structures broaden our current knowledge of the molecular mechanisms of SRP19–SRP RNA and RNA–RNA tertiary interactions and significantly increase the structural SRP database. The comparison of the RNA–RNA tertiary interactions with previous structural data allows a correction of the current SRP-assembly paradigm and the proposal of a new and generalized SRP-assembly scheme.

2. Experimental procedures

2.1. Cloning and purification of SRP RNA

DNA fragments encoding *Sulfolobus solfataricus* (nucleotides 133–228) and human (nucleotides 123–227) SRP RNA were amplified by PCR using primers containing the T7 promoter and were cloned into the pUC18 vector *via* the *Kpn*I/*Xba*I restriction sites and into pUC19 *via* the *Eco*RI/*Xba*I restriction sites, respectively. Oligonucleotides encoding hammerhead ribozymes were ligated directly after the SRP RNA coding region using the *Xba*I/*Hin*dIII restriction sites. The nucleotides at the 5′ and 3′ ends of the SRP RNA were modified according to the requirements for the hammerhead ribozyme (Fig. 1*b*; Price *et al.*, 1995). Plasmids were amplified in *E. coli* DH5α and were purified with the Plasmid Giga Prep Kit (Qiagen). After plasmid linearization with *Hin*dIII, SRP RNAs were produced by runoff *in vitro* transcription and were purified by denaturing polyacrylamide gel electrophoresis and electro elution in 0.25× Tris–borate–EDTA buffer. The purified RNAs were desalted on PD10 columns (GE Healthcare), eluted into water, concentrated to 5–10 mg ml^{-1} in a speedvac and stored at 253 K.

2.2. Cloning and purification of SRP19

A DNA fragment encoding *S. solfataricus* SRP19 with an N-terminal hexahistidine tag directly linked to the protein was amplified by PCR from a genomic DNA preparation and cloned into pET24d *via* the *Nco*I/*Bam*HI restriction sites. SRP19 was expressed in *E. coli* Rosetta (DE3) (Novagen) in the presence of 1 m*M* IPTG at 303 K with vigorous shaking for 12–16 h. Harvested cells were resuspended in ice-cold buffer *A* [20 m*M* Na HEPES, 350 m*M* KCl, 40 m*M* imidazole, 20 m*M* $MgCl_2$, 10 m*M* KCl, 2.5%(*v*/*v*) glycerol pH 8.0]. Cell lysis was performed in an M110L Microfluidizer (Microfludix Inc.) and the lysate was cleared by ultracentrifugation at 91 000*g* for 20 min at 277 K. The supernatant was applied onto a 1 ml Ni–NTA HiTrap column (GE Healthcare) and bound SRP19 was eluted with buffer *B* (buffer *A* supplemented with 460 m*M* imidazole). SRP19-containing fractions were pooled, flash-frozen in liquid nitrogen and stored at 193 K.

Table 1
Data-collection and refinement statistics.

Values in parentheses are for the highest resolution shell.

	Ss SRP19–SRP RNA	*Hs* SRP19–SRP RNA
Data collection		
Beamline (ESRF)	ID14eh2	ID23eh2
Space group	$P2_1$	$P4_32_12$
Unit-cell parameters (Å, °)	a = 71.3, b = 79.3, c = 114.1, β = 102.0	a = 100.3, c = 294.6
No. of complexes per ASU	2	2
Solvent content (%)	67.5	68.5
Resolution (Å)	64.7–3.2 (3.37–3.20)	70.2–3.8† (4.01–3.80)
No. of unique reflections	20578	14852
Multiplicity	3.9 (3.9)	3.0 (3.0)
Completeness (%)	99.2 (99.2)	96.1 (97.9)
$\langle I/\sigma(I)\rangle$	13.6 (3.3)	7.3 (1.3)
$R_{\rm merge}$‡ (%)	9.2 (38.8)	10.3 (60.8)
Refinement		
Resolution (Å)	64.7–3.2	70.2–3.8
No. of reflections	19509	14017
$R_{\rm work}$§/$R_{\rm free}$¶	24.0/28.5	29.1/32.9
No. of atoms	5655	6392
Average B factor (Å^2)	86.7	88.0
R.m.s. deviations		
Bond lengths (Å)	0.015	0.007
Bond angles (°)	1.619	1.352
Ramachandran plot (%)		
Most favoured	75.8	78.0
Additionally allowed	24.2	21.5
Generously allowed	0.0	0.5
Disallowed	0.0	0.0

† The crystal diffracted anisotropically to 3.5 Å. The generous resolution cutoff is the result of a compromise between reasonable completeness and data statistics and (σ_A-weighted) electron-density map quality. ‡ $R_{\rm merge} = \sum_{hkl}\sum_i |I_i(hkl) - \langle I(hkl)\rangle|/\sum_{hkl}\sum_i I_i(hkl)$. § $R_{\rm work} = \sum_{hkl} ||F_{\rm obs}| - k|F_{\rm calc}||/\sum_{hkl}|F_{\rm obs}|$, where k is a scale factor. ¶ $R_{\rm free}$ is $R_{\rm work}$ for 5% of all data that were not used in refinement.

Human SRP19 was cloned and purified as described by Wild *et al.* (2001). The construct was C-terminally truncated by 24 residues and contained a C-terminal hexahistidine tag (linked by a Leu-Glu dipeptide). The original protocol was extended by a heparin chromatography step in the same buffer without imidazole [50 m*M* Tris pH 8.0, 10 m*M* $MgCl_2$, 10 m*M* KCl, 20%(*v*/*v*) glycerol, 0.02%(*v*/*v*) monothioglycerol, 150–800 m*M* NaCl] to improve protein purity. The purified protein was flash-frozen in liquid nitrogen and stored at 193 K.

2.3. Reconstitution of the SRP19–SRP RNA complexes

To obtain the *S. solfataricus* SRP binary complex, SRP RNA was heated for 10 min at 338 K and added stepwise to purified SRP19. The mixture was incubated for 20 min at room temperature. Unbound SRP19 was removed using a MonoQ ion-exchange column (GE Healthcare) in 20 m*M* HEPES pH 8.0, 10–990 m*M* KCl, 20 m*M* $MgCl_2$ and 1.25%(*v*/*v*) glycerol. SRP19–SRP RNA complex-containing fractions were pooled, concentrated (Amicon Ultra, 30 kDa cutoff) and further purified by size-exclusion chromatography (Superdex 200/20–60, GE Healthcare) equilibrated in 20 m*M* HEPES pH 8.0, 200 m*M* KCl and 20 m*M* $MgCl_2$.

For the human SRP19–SRP RNA complex, in a modification of a standard reconstitution protocol (Price *et al.*, 1995) the RNA was heated in the presence of 10 m*M* $MgCl_2$, 10 m*M* KCl and 6 *M* urea for 3 min at 338 K and snap-cooled (at least 20 times dilution) in ice-cold SRP19 (threefold excess) in a buffer consisting of 20 m*M* Tris pH 8.0, 300 m*M* NaCl, 10 m*M* $MgCl_2$, 10 m*M* KCl, 10%(*v*/*v*) glycerol and 0.02%(*v*/*v*) monothioglycerol. After an incubation of 30 min on ice, the complex was applied onto a MonoQ ion-exchange column in the same buffer without glycerol and eluted with an NaCl gradient. The pooled fractions were finally purified by size-exclusion chromatography (Superdex S200 16/60, GE Healthcare) in the same buffer containing 250 m*M* NaCl. For crystallization, the complex was concentrated to >30 mg ml^{-1} and drops were set up immediately.

2.4. Crystallization, data collection and structure determination

The *S. solfataricus* SRP19–SRP RNA complex (in 20 m*M* HEPES pH 8.0, 200 m*M* KCl and 20 m*M* $MgCl_2$, concentration of >10 mg ml^{-1}) was crystallized manually at 293 K by the hanging-drop technique (1 + 1 µl drops) over a reservoir (1 ml) consisting of 100 m*M* cacodylate pH 5.7, 400 m*M* KCl, 10 m*M* $CaCl_2$ and 15%(*w*/*v*) PEG 4000. Crystals appeared within one week. Prior to data collection, crystals were flash-frozen in liquid nitrogen.

The human binary complex was crystallized in the buffer that was used for purification [20 m*M* Tris pH 8.0, 250 m*M* NaCl, 10 m*M* $MgCl_2$, 10 m*M* KCl and 0.02%(*v*/*v*) monothioglycerol] by the sitting-drop technique: drops were set up using a nano-dispensing robot (Phoenix, Art Robbins), mixing 200 nl complex solution with 100 nl reservoir solution, and were equilibrated against 100 µl reservoir solution at 291 K. The optimized conditions were 0.75 *M* potassium fluoride, 2.2 *M* ammonium sulfate and 100 m*M* sodium acetate pH 4.5. Crystals appeared after 3 d and grew to maximal dimensions of 180 × 100 × 100 µm within one week. For data collection, the crystals were quickly dipped in reservoir solution supplemented with 20%(*v*/*v*) glycerol before being flash-frozen in liquid nitrogen.

All data collection for the crenarchaeal and human complexes was performed at the European Synchrotron Radiation Facility (ESRF) in Grenoble, France. Molecular replacement was performed with the program *Phaser* (Read, 2001) within the *CCP*4 suite (Collaborative Computational Project, Number 4, 1994; see §3 for details). For refinement we used *REFMAC*5 (Murshudov *et al.*, 1997). The rather low-resolution human structure was only refined by rigid-body adjustments of the human ternary complex and local idealization of the model geometry performed with *Coot* (Emsley & Cowtan, 2004). In a last round the model was optimized (drops in R and $R_{\rm free}$ of more than 5%) by individual refinement with almost constrained model geometry (geometric weight within *REFMAC*5 of 0.01), applying a simple anisotropic scaling procedure without bulk-solvent correction in order to avoid possible overfitting of the data and to obtain a reasonable overall temperature factor. Structure factors and coordinates have been deposited in the Protein Data Bank under accession codes 3ktw for the *S. solfataricus* binary complex and 3ktv for the human binary complex.

3. Results

3.1. Overview of the structures

The crenarchaeal (*S. solfataricus*; *Ss*) SRP19 was cocrystallized with a 96-nucleotide fragment of SRP RNA comprising most of the SRP S domain. The crystals belonged to the monoclinic space group $P2_1$ and diffracted to 3.0 Å resolution. The crystals of the human (*Hs*) complex with a corresponding SRP RNA of 105 nucleotides belonged to the tetragonal space group $P4_32_12$. Owing to a long cell axis and weak diffraction to 3.8 Å resolution (anisotropically to 3.5 Å resolution), the data for the latter had to be collected on the high-brilliance beamline ID23-1 and the microfocus beamline ID23-2 at the European Synchrotron Radiation Facility (ESRF) in Grenoble, France. All data and refinement statistics are given in Table 1 and sequences and structures are depicted in Fig. 1. Both structures were solved by molecular replacement using the archaeal *M. jannaschii* (*Mj*) binary complex (PDB code 1lng; Hainzl *et al.*, 2002) and the all-human binary complex as taken from the SRP19–SRP54M–SRP RNA complex (PDB code 1mfq; termed in the following as the ternary complex; Kuglstatter *et al.*, 2002) as search models, respectively. Interestingly, all attempts to use the heterologous structure of *Mj* SRP19 bound to human SRP RNA (Oubridge *et al.*, 2002) as a search model for the human complex failed, indicating significant structural differences. Indeed, the r.m.s. deviations between the SRP RNAs are 2.3 Å (human binary *versus* human ternary), whereas the r.m.s. deviation is 4.7 Å between the human and the heterologous binary complex. Differences between the all-human complexes are mainly restricted to the long strand of the asymmetric loop, which was therefore omitted from the model and rebuilt (Fig. 2), and the orientation of RNA helix 5 with respect to helices 6–8 (Fig. 3*c*). In contrast, in the heterologous binary complex the relative orientation of SRP19 to SRP RNA and the SRP RNA itself are different (Fig. 3*b*), as described in detail in the comparison with the human ternary structure (Kuglstatter *et al.*, 2002).

In both the human and crenarchaeal binary complexes the SRP RNA has an approximate Y-shape with SRP19 bound to both apices of the Y. The RNA includes most of the S-domain SRP RNA with the entire helices 6–8 and parts of helix 5 (5′ and 3′ ends; Fig. 1*b*). Helices 5, 6 and 8 are connected *via* a three-way junction involving a classical U-turn at the 3′ end of helix 6. Helices 5 and 8 are coaxially stacked. Helices 6 and 8 are juxtaposed and are capped by tetranucleotide hairpin loops (tetraloops) that interact with each other as described previously (Oubridge *et al.*, 2002; Hainzl *et al.*, 2002).

SRP19 in mammalia and archaea is a small RNA-binding protein with a $\beta\alpha\beta\beta\alpha$ topology (Figs. 1*b* and 1*c*; Wild *et al.*, 2001). More than half of the protein is not involved in secondary structure and the human protein is not stable in solution (T_m below 313 K; data not shown). In contrast, archaeal SRP19 is a stable protein with reduced loop sizes (especially loop L4 before helix α2; loop definitions are according to the first SRP19 structure; Wild *et al.*, 2001). This also applies to *Ss* SRP19 as presented here in the context of the binary complex (Figs. 1*b* and 1*c*). Although the sequence conservation in the SRP19 family is in general low (*e.g.* 21.5% between *Ss* and *Hs* SRP19 and 33% between *Ss* and *Mj* SRP19; Fig. 1*c*), the structural deviations between all SRP19 structures are small (in the r.m.s.d. range of 2 Å). The similarities also extend over the long L1 and L3 loops. A special feature of *Ss* SRP19 is an additional N-terminal helix and a reduced L1 size.

3.2. Protein–RNA interactions

SRP19 recognizes the SRP RNA both by secondary structure elements and by extended loop regions. The total inter-

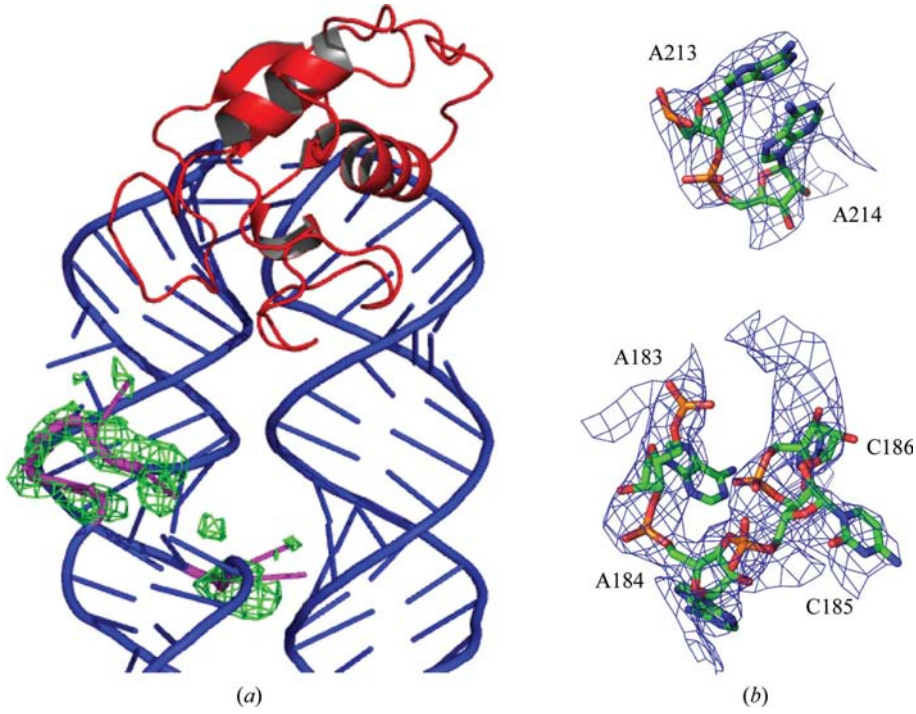

Figure 2
Electron-density maps for the human SRP19–SRP RNA complex. (*a*) Unbiased $mF_o - DF_c$ difference electron-density map contoured at the 3σ level for the asymmetric loop of SRP RNA helix 8 based on the initial model of the human ternary complex without the asymmetric loop. The density (green) is shown together with the final model (asymmetric loop in magenta). The conformation of the long strand of the asymmetric loop is different to that of the ternary complex and was rebuilt. (*b*) Final $2mF_o - DF_c$ map for the asymmetric loop contoured at the 1.5σ level. The trace of the phosphoribose backbone is unambiguous and only the position of the base of A183 is not clearly defined.

face is 1050 Å^2 (buried surface of 2100 Å^2) for human SRP and 1350 Å^2 for the crenarchaeal SRP. SRP19 mainly resides at the apex of RNA helix 6 and contacts the phosphoribose side of the GNAR tetraloop (where N is any nucleotide and R is a purine nucleotide; Wild *et al.*, 2001; Oubridge *et al.*, 2002; Hainzl *et al.*, 2002; Kuglstatter *et al.*, 2002).

Although the SRP19–SRP RNA interactions are similar in the systems studied to date, an interesting structural difference exists. In *Mj* SRP the distal stem of helix 6 has an increased helical rise with respect to the human system, which results in a more shallow major groove and a register shift by one base in the SRP19 L1 loop–helix 6 interaction (Hainzl *et al.*, 2002). However, the register shift is not present in the crenarchaeon *S. solfataricus* and the helical rise is therefore not increased. Instead, *Ss* SRP19 is rotated into the groove, which shifts helix α2 by up to 4 Å and therefore maintains the tight binding to the RNA (Fig. 3*a*). To accommodate the rotation without clashing into the RNA, *Ss* SRP19 L1 is shortened by two residues with respect to the *Mj* and *Hs* SRP19s (Fig. 1*c*).

3.3. RNA–RNA tertiary interactions

Two sites of RNA–RNA tertiary interactions are found between helices 6 and 8 (Oubridge *et al.*, 2002; Hainzl *et al.*, 2002; Fig. 1*b*). The first site comprises the unique interaction between the two helix-capping tetraloops, with their two conserved adenosines forming a symmetrical base pair. A second site of tertiary interactions includes the asymmetric loop in helix 8 interacting with helix 6. Here, mammalian and archaeal SRP differ in their structural organization. In the human SRP ternary complex (Kuglstatter *et al.*, 2002) two unpaired adenosines (A213-A214) bulge out from the short strand of the asymmetric loop and form A-minor motifs with a completely stacked helix 6 (Fig. 4*c*; bulged-out loops are termed in the following as the 'out' conformation). In contrast, in the *Mj* SRP S-domain structures (Hainzl *et al.*, 2007) two unpaired adenosines (A176-A177) in the distal strand of helix 6 are bulged out and interact in the minor groove of helix 8 with a continuously base-paired short strand of the loop (Figs. 4*d*–4*f*).

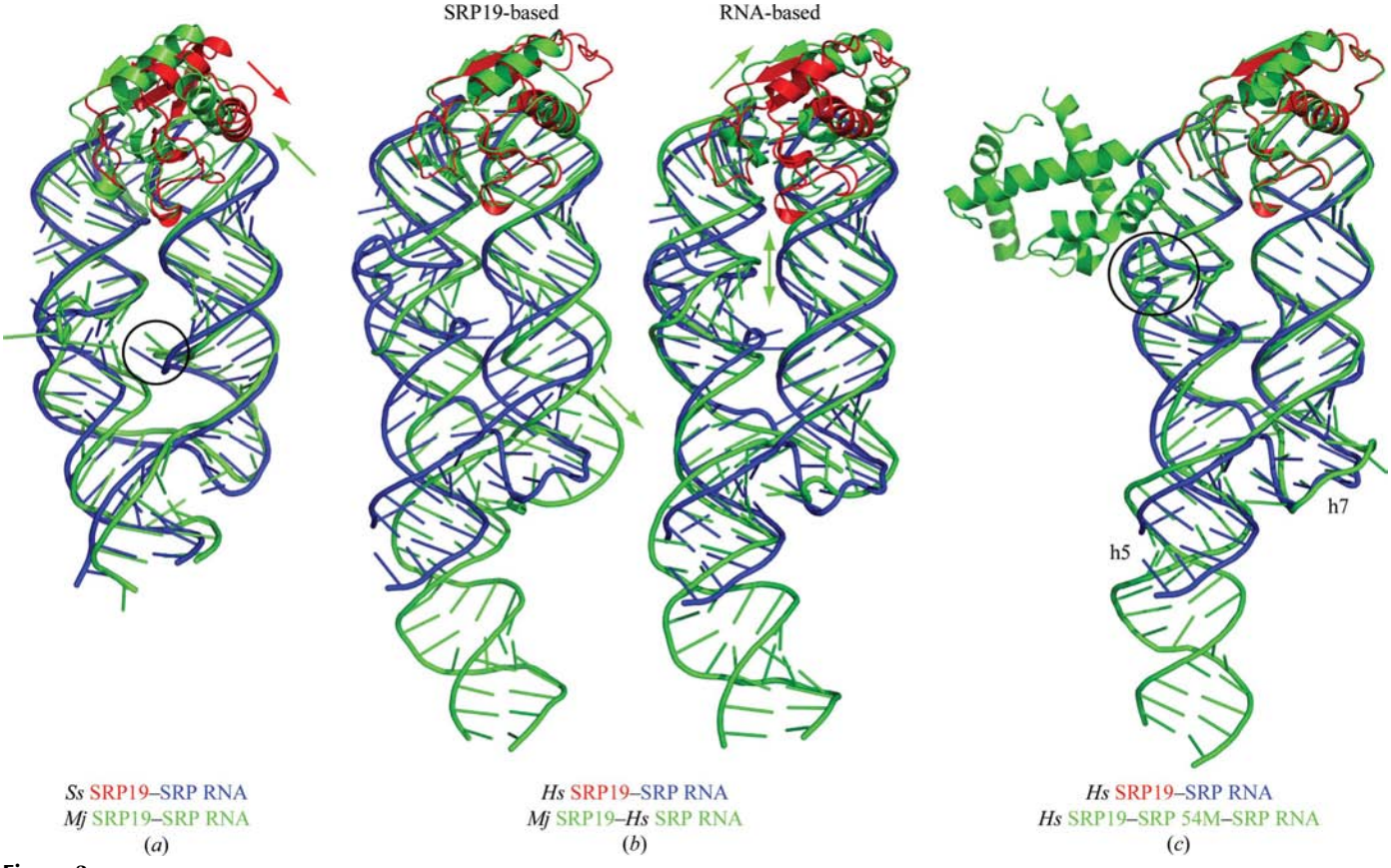

Figure 3
Superpositions of SRP S-domain structures. (*a*) Superposition of archaeal SRP19–SRP RNA binary complexes. That from *S. sulfolobus* is shown in blue and red and that from *M. jannnaschii* is shown in green only (PDB code 1lng). While *Mj* SRP RNA shows an increased rise of helix 6 next to the tetraloop (green arrow), *Ss* SRP19 is rotated into the major groove (red arrow) to maintain a tight protein–RNA interface. In both structures the asymmetric loop is bulged out and RNA–RNA tertiary interactions are formed (encircled). (*b*) Superpositions of the all-human binary complex (blue/red) with the heterologous *Mj* SRP19–human SRP RNA structure (PDB code 1l9a, green; Oubridge *et al.*, 2002). The orientation and conformation of SRP RNA differs significantly. The asymmetric loop is not collapsed and RNA–RNA tertiary interactions are not formed in the heterologous structure. Major differences are indicated by green arrows. (*c*) Superposition of the human binary (blue/red) and ternary complexes (PDB code 1mfq, green). The two complexes superpose well, with the exceptions of the longer strand of the asymmetric loop (encircled), the conformation of helix 7 and the position of helix 5 (labelled).

Interestingly, the RNA–RNA tertiary interactions in the human binary SRP19–SRP RNA structure reported here correspond to the ternary complex including SRP54M (Figs. 4*b* and 4*c*). The two adenosines comprising the short strand of the asymmetric loop are bulged out and form the described A-minor motifs. This observation is in contrast to the reported heterologous *Mj* SRP19–human SRP RNA structure (Oubridge *et al.*, 2002; Fig. 4*a*), which has been taken as a model for the all-human binary complex and in which the two bases are stacked into the helix (referred to in the following as the 'in' conformation). The 'out' conformation of the two adenosines enables a collapse of the asymmetric loop in comparison to the heterologous binary complex, which results in expulsion of the long strand of the loop (Fig. 4*b*). However, the arrangement of the four exposed nucleotides (183-AACC) is different from the human ternary complex, in which the bases of the loop stack continuously and form a platform for SRP54M that is almost perpendicular to the RNA helical axis (Fig. 4*c*). In the binary complex no stacking is observed and the base positions, although irregular and not well defined owing to the resolution limit, are stabilized by crystal contacts. The fact that the loop is stabilized by crystal contacts raises the question of whether the bulged-out conformation might be influenced by the crystal packing. This would be difficult to answer if the overall RNA conformation in the known heterologous 'in' structure and the human ternary 'out' structure were the same; however, this is not the case (Fig. 3). The overall RNA conformation we observe is almost identical to the ternary complex (although the crystal form is different) and the RNA as observed in the heterologous (uncollapsed) structure would not fit into our crystalline array. Therefore, we conclude that the 'out' conformation in our structure is not a consequence of crystal packing but rather of the general overall conformation of the RNA itself. This conclusion is supported by the fact that the loops of the two independent RNA molecules within the crystallographic asymmetric unit are in different crystalline environments.

In the crenarchaeal *Ss* SRP binary complex, similar to *Mj* SRP, RNA–RNA tertiary interactions involve a bulge within helix 6 adjacent to the asymmetric loop of helix 8 (Fig. 4*g*). Here, an unpaired uridine (U179) flips out from helix 6 and interacts with the minor groove and the short strand of helix 8 (G224), which is completely stacked. The long strand of the asymmetric loop is bulged out, but in contrast to other known binary complexes only two nucleotides are exposed (A197-C198) and form a stacked platform even in the absence of

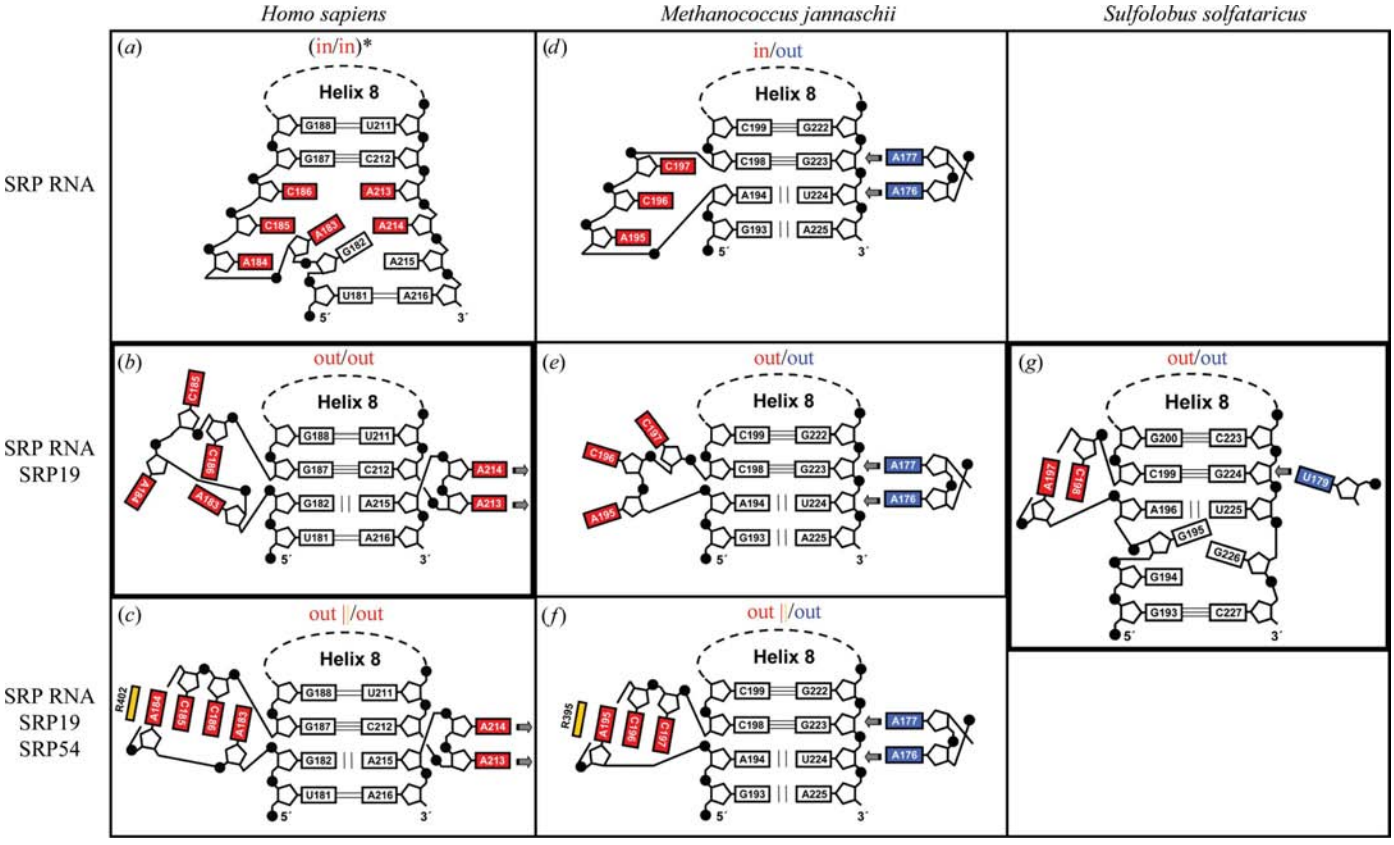

Figure 4
The asymmetric loop of SRP RNA helix 8. The conformations of the asymmetric loops (red) are given for the human (*a*, *b*, *c*) and known archaeal structures (*d*, *e*, *f*, *g*) in the free, SRP19-bound and SRP19/SRP54-bound contexts. The structures reported here are boxed with bold lines. Nucleotides from helix 6 involved in tertiary interactions (grey arrows) are given in blue and a conserved arginine residue from SRP54M stacking on the RNA platform is drawn in yellow. The different loop conformations are indicated by 'in' for stacked and 'out' for solvent-exposed. The platform within the long strand of the asymmetric loop is emphasized by the '||' symbol. Free human SRP RNA is modelled (denoted by an asterisk) from the heterologous *Mj* SRP19–human SRP RNA complex in accordance with chemical footprint data (Menichelli *et al.*, 2007; Rose & Weeks, 2001).

SRP54. Although the loop is stabilized by crystal contacts, which are different for the two molecules of the asymmetric unit, the stacked conformation is maintained in both molecules. However, the loop conformation is different to the *Ss* SRP54–helix 8 structure (Rosendal *et al.*, 2003), which was solved at 4 Å resolution and in which the base positions are therefore only poorly defined.

4. Discussion

The structures of binary complexes of SRP19 bound to S-domain SRP RNA have been solved for a crenarchaeal and the human SRP system. The structures complement the archaeal structure known from *M. jannaschii* (Hainzl *et al.*, 2002) and replace the heterologous *M. jannaschii* SRP19–human SRP RNA structure (Oubridge *et al.*, 2002) that has been used as a model for the all-human complex. The overall structures of the three homologous binary complexes are highly similar and highlight the importance of SRP19 for stabilizing the SRP RNA fold. SRP19 is known to induce (mammalia) and lock (mammalia and archaea) the side-by-side alignment of RNA helices 6 and 8 and thereby enables the structural changes within the asymmetric loop of helix 8 that are necessary for SRP54 recruitment. However, mammalia and archaea have evolved different mechanisms for RNA–RNA tertiary interactions (Figs. 4 and 5). Whereas in human SRP, and likely in other mammals and eukaryotes, RNA–RNA tertiary interactions are formed by bases looping out from helix 8, in archaea they seem to be provided from the opposite side bulging out from helix 6, as demonstrated by the presented crenarchaeal structure and the known *M. jannaschii* structures (Fig. 4). This principle is supported by comparative sequence alignments (Rosenblad *et al.*, 2003), which show that the distal strand of the asymmetric loop is elongated by a single nucleotide (usually an adenosine) in eukaryotic SRP. In order to form the binding platform for SRP54 comprising the proximal strand of the loop, the entire loop needs to collapse as shown for human SRP (Kuglstatter *et al.*, 2002). For this to occur, the two non-base-paired nucleotides from the distal strand have to be expelled from the helix. Only then can the distal strand continuously stack within helix 8, as is the case for all SRP RNAs studied so far. In archaea (and bacteria) the distal strand is shorter, the collapse does not occur and all bases remain stacked into the helix.

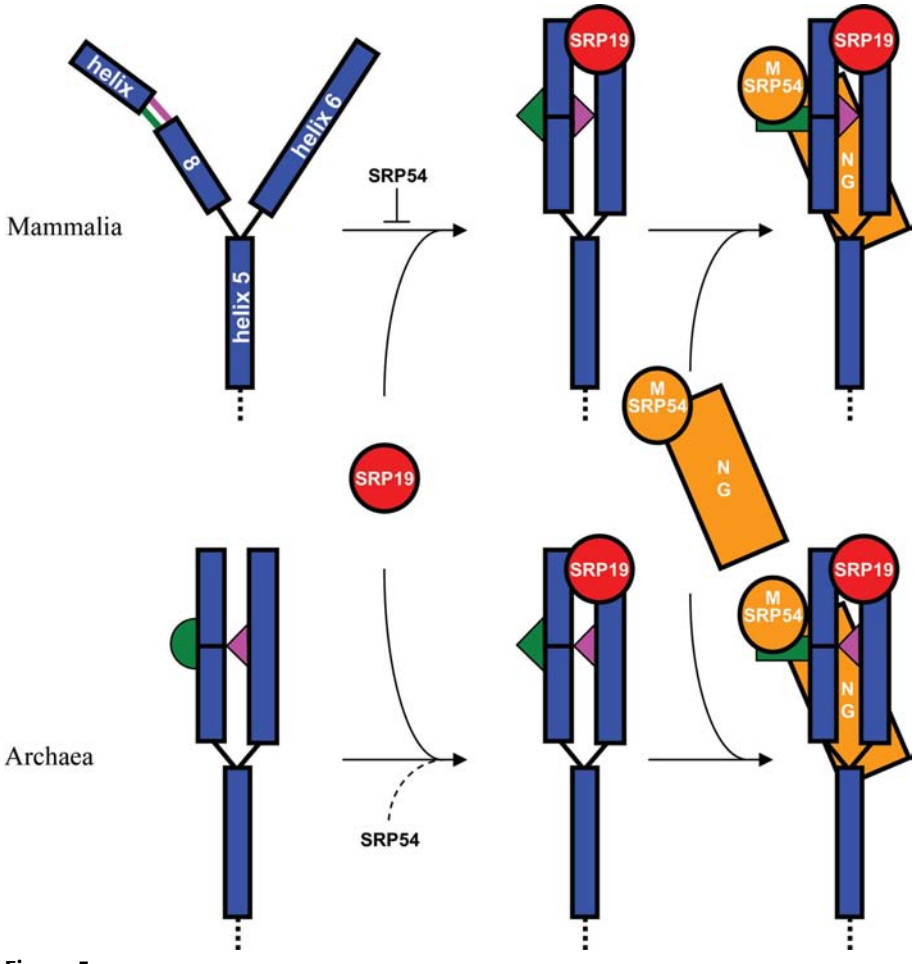

Figure 5
Changes within SRP RNA during assembly with SRP19 and SRP54. In mammalia (top row) free SRP RNA is flexible, the asymmetric loop (green and magenta) in helix 8 is not collapsed and SRP54 can only bind after SRP19 has juxtaposed helices 6 and 8. In contrast, in archaea free SRP RNA and the asymmetric loop are already primed for SRP54 binding, collapse of the asymmetric loop does not occur and bases from helix 6 are bulged out to form RNA–RNA tertiary interactions.

How could such a collapse be induced? Is it an intrinsic property of the RNA or does it require binding of SRP19 and/or SRP54? Archaeal SRP RNA binds SRP54 even in the absence of SRP19 (Tozik *et al.*, 2002; Maeshima *et al.*, 2001; Bhuiyan *et al.*, 2000). Although binding is significantly weaker than in the presence of SRP19, this property marks a clear difference from the mammalian SRP (Walter & Blobel, 1983) and resembles the bacterial situation. In the current assembly paradigm using the heterologous *Mj* SRP19–human SRP RNA structure as a mammalian prototype it has been stated that SRP19 is not able to induce the collapsed conformation of the asymmetric loop of helix 8 in the mammalian binary complex. However, the structure of the all-human SRP19–SRP RNA complex presented here shows that this is clearly not the case and that the asymmetric loop is in a collapsed 'out/out' conformation (Fig. 4). The reason for the observed structural discrepancy might lie in the increase in the helical rise of RNA helix 6 as induced by *Mj* SRP19, which results in a lengthening of RNA helix 8 and a register shift by one base in the SRP19–SRP RNA helix 6 interaction (right panel of Fig. 3*b*).

As the asymmetric loop conformations in the mammalian and archaeal binary complexes are therefore highly similar, the observed differences in the assemblies have to be attributed to the SRP RNA itself (as summarized in a new SRP-assembly scheme in Fig. 5). This idea is supported by the finding that archaeal SRP RNA can bind human SRP54M even in the absence of SRP19 (Bhuiyan *et al.*, 2000), while human SRP RNA cannot. The crystal structure of *Mj* SRP RNA alone (Hainzl *et al.*, 2005) and RNase protection data (Yin *et al.*, 2004) show that in the absence of SRP19 RNA helices 6 and 8 are properly aligned in archaea and the RNA–RNA tertiary interactions are already formed. Therefore, the long strand of the asymmetric loop is available to SRP54 at least to some extent and assembly can occur. This is not the case for the mammalian SRP RNA and without any protein bound the helices swing away from each other as shown by α-sarcin cleavage and chemical footprinting data (Diener & Wilson, 2000; Rose & Weeks, 2001; Siegel & Walter, 1988). Moreover, in the free form the bases of the asymmetric loop are likely to be stacked into helix 8 as the collapse does not occur and the two adenine bases are not available to stabilize the RNA–RNA tertiary interactions as observed in the heterologous structure (Oubridge *et al.*, 2002). Only in the presence of (mammalian) SRP19 are the helices stably juxtaposed; the asymmetric loop collapses and exposes the bases from the long strand of the asymmetric loop, which subsequently forms the binding platform for SRP54. The conclusion drawn by our crystallographic data is supported by recent chemical and enzymatic probing (Menichelli *et al.*, 2007), which shows that the presence of SRP19 together with SRP68/72 is indeed sufficient to induce the collapse.

The exact mechanism of the collapse remains elusive, as SRP19 binds to the apices of SRP RNA helices 6 and 8 and does not contact the asymmetric loop itself. Possible explanations for the collapse might be the compression of helix 8 and/or chemical attraction induced by the helical juxtaposition. The assembly of this ribonucleoprotein particle and even of this single step is therefore still far from being understood.

We thank the European Synchrotron Radiation Facility (ESRF, Grenoble, France) for access to the beamlines and their staff for excellent technical assistance. We gratefully acknowledge the contributions of K. Stengel and S. Ravaud in the early stages of the project. We thank A. Meinhart for stimulating ideas on human SRP19 stability. This work was supported by the Deutsche Forschungsgemeinschaft collaboration project grant SFB638 to IS and by a Boehringer Ingelheim Fonds predoctoral fellowship to G. Bozkurt.

References

Batey, R. T., Rambo, R. P., Lucast, L., Rha, B. & Doudna, J. A. (2000). *Science*, **287**, 1232–1239.
Batey, R. T., Sagar, M. B. & Doudna, J. A. (2001). *J. Mol. Biol.* **307**, 229–246.
Bhuiyan, S. H., Gowda, K., Hotokezaka, H. & Zwieb, C. (2000). *Nucleic Acids Res.* **28**, 1365–1373.
Bradshaw, N., Neher, S. B., Booth, D. S. & Walter, P. (2009). *Science*, **323**, 127–130.
Collaborative Computational Project, Number 4 (1994). *Acta Cryst.* D**50**, 760–763.
Cross, B. C., Sinning, I., Luirink, J. & High, S. (2009). *Nature Rev. Mol. Cell Biol.* **10**, 255–264.
Diener, J. L. & Wilson, C. (2000). *Biochemistry*, **39**, 12862–12874.
Egea, P. F., Shan, S. O., Napetschnig, J., Savage, D. F., Walter, P. & Stroud, R. M. (2004). *Nature (London)*, **427**, 215–221.
Egea, P. F., Stroud, R. M. & Walter, P. (2005). *Curr. Opin. Struct. Biol.* **15**, 213–220.
Emsley, P. & Cowtan, K. (2004). *Acta Cryst.* D**60**, 2126–2132.
Focia, P. J., Shepotinovskaya, I. V., Seidler, J. A. & Freymann, D. M. (2004). *Science*, **303**, 373–377.
Grudnik, P., Bange, G. & Sinning, I. (2009). *Biol. Chem.* **390**, 775–782.
Hainzl, T., Huang, S. & Sauer-Eriksson, A. E. (2002). *Nature (London)*, **417**, 767–771.
Hainzl, T., Huang, S. & Sauer-Eriksson, A. E. (2005). *RNA*, **11**, 1043–1050.
Hainzl, T., Huang, S. & Sauer-Eriksson, A. E. (2007). *Proc. Natl Acad. Sci. USA*, **104**, 14911–14916.
Halic, M., Blau, M., Becker, T., Mielke, T., Pool, M. R., Wild, K., Sinning, I. & Beckmann, R. (2006). *Nature (London)*, **444**, 507–511.
Jacobson, M. R. & Pederson, T. (1998). *Proc. Natl Acad. Sci. USA*, **95**, 7981–7986.
Kuglstatter, A., Oubridge, C. & Nagai, K. (2002). *Nature Struct. Mol. Biol.* **9**, 740–744.
Luirink, J. & Sinning, I. (2004). *Biochim. Biophys. Acta*, **1694**, 17–35.
Maeshima, H., Okuno, E., Aimi, T., Morinaga, T. & Itoh, T. (2001). *FEBS Lett.* **507**, 336–340.
Maity, T. S., Leonard, C. W., Rose, M. A., Fried, H. M. & Weeks, K. M. (2006). *Biochemistry*, **45**, 14955–14964.
Maity, T. S. & Weeks, K. M. (2007). *J. Mol. Biol.* **369**, 512–524.
Menichelli, E., Isel, C., Oubridge, C. & Nagai, K. (2007). *J. Mol. Biol.* **367**, 187–203.
Murshudov, G. N., Vagin, A. A. & Dodson, E. J. (1997). *Acta Cryst.* D**53**, 240–255.
Nagai, K., Oubridge, C., Kuglstatter, A., Menichelli, E., Isel, C. & Jovine, L. (2003). *EMBO J.* **22**, 3479–3485.
Oubridge, C., Kuglstatter, A., Jovine, L. & Nagai, K. (2002). *Mol. Cell*, **9**, 1251–1261.
Politz, J. C., Yarovoi, S., Kilroy, S. M., Gowda, K., Zwieb, C. & Pederson, T. (2000). *Proc. Natl Acad. Sci. USA*, **97**, 55–60.
Price, S. R., Ito, N., Oubridge, C., Avis, J. M. & Nagai, K. (1995). *J. Mol. Biol.* **249**, 398–408.
Read, R. J. (2001). *Acta Cryst.* D**57**, 1373–1382.
Rose, M. A. & Weeks, K. M. (2001). *Nature Struct. Mol. Biol.* **8**, 515–520.
Rosenblad, M. A., Gorodkin, J., Knudsen, B., Zwieb, C. & Samuelsson, T. (2003). *Nucleic Acids Res.* **31**, 363–364.
Rosendal, K. R., Wild, K., Montoya, G. & Sinning, I. (2003). *Proc. Natl Acad. Sci. USA*, **100**, 14701–14706.
Sauer-Eriksson, A. E. & Hainzl, T. (2003). *Curr. Opin. Struct. Biol.* **13**, 64–70.
Schmitz, U., Behrens, S., Freymann, D. M., Keenan, R. J., Lukavsky, P., Walter, P. & James, T. L. (1999). *RNA*, **5**, 1419–1429.
Siegel, V. & Walter, P. (1986). *Nature (London)*, **320**, 81–84.
Siegel, V. & Walter, P. (1988). *Proc. Natl Acad. Sci. USA*, **85**, 1801–1805.
Tozik, I., Huang, Q., Zwieb, C. & Eichler, J. (2002). *Nucleic Acids Res.* **30**, 4166–4175.
Walter, P. & Blobel, G. (1983). *Cell*, **34**, 525–533.
Weichenrieder, O., Wild, K., Strub, K. & Cusack, S. (2000). *Nature (London)*, **408**, 167–173.
Wild, K., Sinning, I. & Cusack, S. (2001). *Science*, **294**, 598–601.
Yin, J., Huang, Q., Pakhomova, O. N., Hinck, A. P. & Zwieb, C. (2004). *Archaea*, **1**, 269–275.